Rev. Adv. Mater. Sci. 45 (2016) 42-51

ELASTIC MODULUS, MICROPLASTIC PROPERTIES AND DURABILITY OF TITANIUM ALLOYS FOR BIOMEDICAL APPLICATIONS

V.I. Betekhtin[1], Yu.R. Kolobov[2, 3], O.A. Golosova[4], J. Dvorak[5], V. Sklenicka[5], B.K. Kardashev[1], A.G. Kadomtsev[1], M.V. Narykova[1] and M.B. Ivanov[2]

[1]Ioffe Physical Technical Institute, Russian Academy of Sciences, 26 Politekhnicheskaya St., St. Petersburg 194021, Russia
[2]Belgorod Research University, 85 Pobedy St., Belgorod 308015, Russia
[3]Institute of Problems of Chemical Physics, Russian Academy of Sciences, 1 Academician Semenov Ave., Chernogolovka 142432, Russia
[4]Institute of Structural Macrokinetics and Materials Science, Russian Academy of Sciences, 8 Academician Osipyan St., Chernogolovka 142432, Russia
[5]Institute of Physics of Materials Academy of Sciences of Czech Republic, 22 Zizkova, 616 62 Brno, Czech Republic

Received: February 18, 2016

Abstract. This research was focused on a new low-modulus β-type titanium alloy Ti–26Nb–7Mo–12Zr (wt.%). The microstructure effects on elastic modulus (measured by the acoustic resonance method) as well as microplastic, mechanical, tribological, and corrosive properties of Ti–26Nb–7Mo–12Zr alloy after thermomechanical processing were examined. The microstructure was characterized in detail by scanning electron microscopy and electron backscatter diffraction methods. The experimental research results have shown that formation of the fully recrystallized structure in the titanium alloy leads to an increase in elastic modulus, microplastic flow stress and plasticity, as compared to the corresponding characteristics of the alloy having partially recrystallized and coarse-grained structures. The durability of β titanium alloy was examined and compared with that of commercially pure α titanium (CP Ti). It was found that, in the same creep loading conditions, the low-modulus Ti–26Nb–7Mo–12Zr alloy exhibits a longer time to creep fracture, as compared to the pure α titanium.

1. INTRODUCTION

Biomaterials used in biomedical applications offer a wide range of adaptable structures for the use in a variety of clinical and scientific cases. Recent enormous demands and development of medical implantations require the creation of new materials for implants that will enhance survival and reliability. Such materials used for implants need an enhanced biochemical compatibility with body tissues (lack of immune reactions and inflammatory processes) and biomechanical compatibility, which is primarily associated with nearly equal values of elastic modulus for implant and bone tissues. This determines the functional reliability of implants [1-5]. The main characteristic of the biomechanical compatibility of an implanted material is the elastic modulus. It is desirable to achieve the elastic modulus close to that corresponding to bone tissue (30 GPa) [5-7]. The low elastic modulus would allow to avoid a stress shielding effect in bone fixation, which would probably cause excessive bone absorption because of decreased mechanical stimulation of the part of the bone replaced with metallic medical devices [6,8,9].

Corresponding author: Yu.R. Kolobov, e-mail: Kolobov@bsu.edu.ru

Among metallic materials, titanium and its alloys are considered the most suitable materials for biomedical applications due to their unique combination of mechanical properties, excellent corrosion resistance and superior biocompatibility [1,3,6,10-14]. The corrosion resistance of titanium and its alloys is significantly higher than that of stainless steel and Cr–Co alloys due to the quick formation of natural passive oxide film on its surface, which is firmly connected with basic metal and excludes the contact of metal with a corrosive active medium [1,15]. An extremely favorable factor of titanium alloys used for the manufacture of implants and prostheses is their low (about two times less than that of steel) modulus of elasticity, which improves the biomechanical compatibility with body tissues. The elastic modulus of β-type titanium alloys is noticeably lower than that of α-type titanium (CP Ti) and (α + β)-type alloys [1,6,18-18]. Therefore, low modulus β-type alloys have been extensively developed to alleviate the stress shielding effect [19,20].

A new β titanium alloys system Ti–Nb–Mo–Zr developed by the authors [21] together with Prof. A.A. Zisman has a low elastic modulus and does not contain cytotoxic elements, such as Al and V, which may cause allergic reaction in living tissues or a general toxic effect in the body [1, 22-26]. Theoretical calculations of the choice of a new low modulus β titanium alloy based on the d-electron alloy design method [27] was reported earlier in [21]. The use of this method allows one to develop alloys based on titanium [28,29], cobalt [30], and nickel [31-33] with desired physico-mechanical properties. The electronic structure of complex-alloying titanium alloy is characterized by two parameters: a degree of the covalent bond (bond order B_o) between titanium and the alloying element and a metal d-orbital energy level (M_d). Values of B_o and M_d have a great influence on various properties of alloys including mechanical, corrosion properties and elastic modulus. According to [21], the desired level of elastic modulus E = 65 GPa is achieved in the area of $2.860 \le B_o \le 2.885$. The alloy composition must also correspond to $2.43 \le M_d \le 2.48$ for the optimal mechanical properties of biomedical materials. These requirements are easily realized in the alloying system of titanium by the following elements: Nb, Mo, and Zr. The experimental melting of titanium alloys system Ti–Nb–Mo–Zr was carried out at the production centre of the VSMPO-AVISMA Corporation (Verkhnyaya Salda, Russia). Ingots were produced by triple vacuum arc remelting and subsequent forging at temperatures above the recrystallization temperature.

It is known that the grain size which determines the level of structure-sensitive mechanical properties is an important characteristic of metals and alloys. The formation of a homogeneous fine-grained, ultrafine-grained, submicrocrystalline or nanostructured states could be expected to provide a significant improvement in physical and mechanical properties. In this context, we formed the homogeneous fine-grained structure in Ti-26Nb-7Mo-12Zr alloy by sheet rolling and subsequent recrystallization annealing. Sheet rolling was carried out without heating at room temperature with a reduction of 100–200 μm in one pass with a total strain of 30, 60 and 90%. Deformed specimens after rolling were annealed at 850 °C and then quenched in water.

2. LOW MODULUS Ti–26Nb–7Mo–12Zr ALLOY: STRUCTURE, ELASTIC AND MICROPLASTIC PROPERTIES

Fig. 1 shows the microstructure of the Ti-26Nb-7Mo-12Zr forged ingot. The alloy is fully β-phase with an average grain size ~ 280 μm in the initial (forged) state. After thermomechanical treatment of the forged alloy, the microstructure was characterized by scanning electron microscope Quanta 600 FEG equipped with a field emission gun. Investigation of the structural phase state and crystallographic texture was also performed by using a method of automatic analysis of electron backscattered diffraction patterns (EBSD) on the scanning electron microscope Quanta 600 FEG. As noted earlier [34], the alloy with a total deformation degree of about 30 (state 1) and 60% (state 2) after annealing (see Figs. 2 and 3) has a partially recrystallized structure. A volume fraction of recrystallized grains (V_{RG}) were 43 and 94%, respectively (Table 1). According to

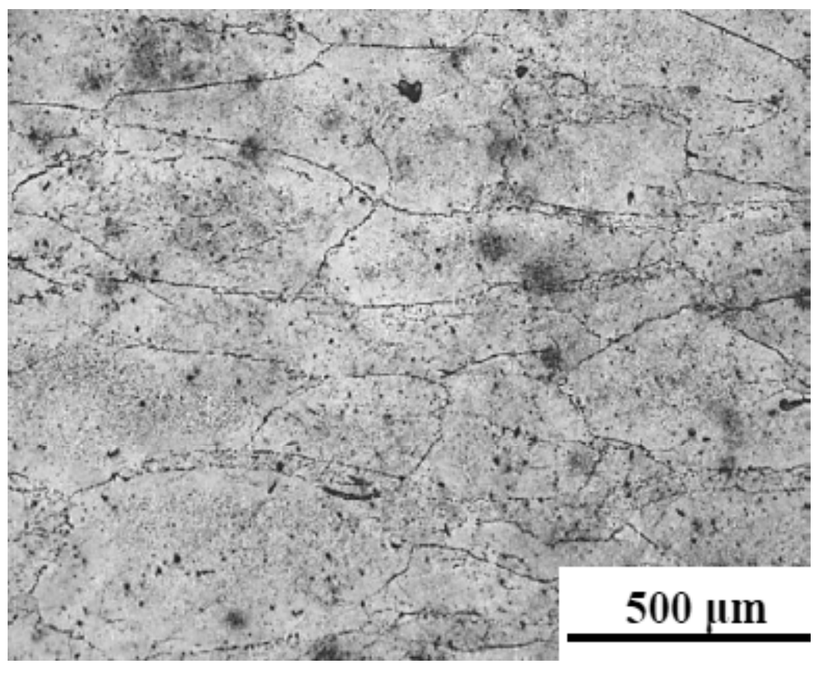

Fig. 1. Microstructure of Ti–26Nb–7Mo–12Zr alloy. Optical metallography.

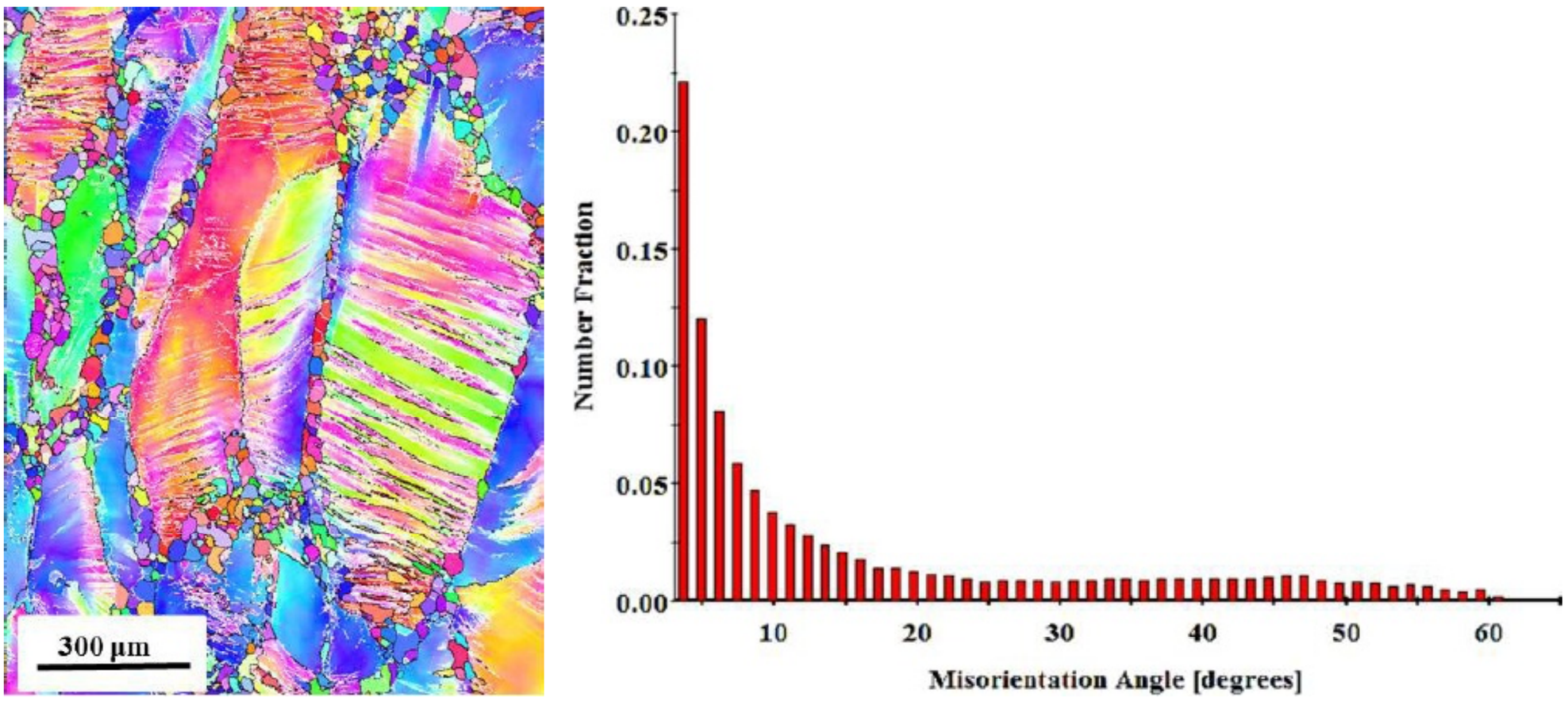

Fig. 2. EBSD grain map (high and low angle grain boundaries are identified by black and white markers, respectively) and the grain boundary misorientation distribution for Ti–26Nb–7Mo–12Zr alloy after rolling at 30% reduction and subsequent annealing at T = 850 °C before quenching.

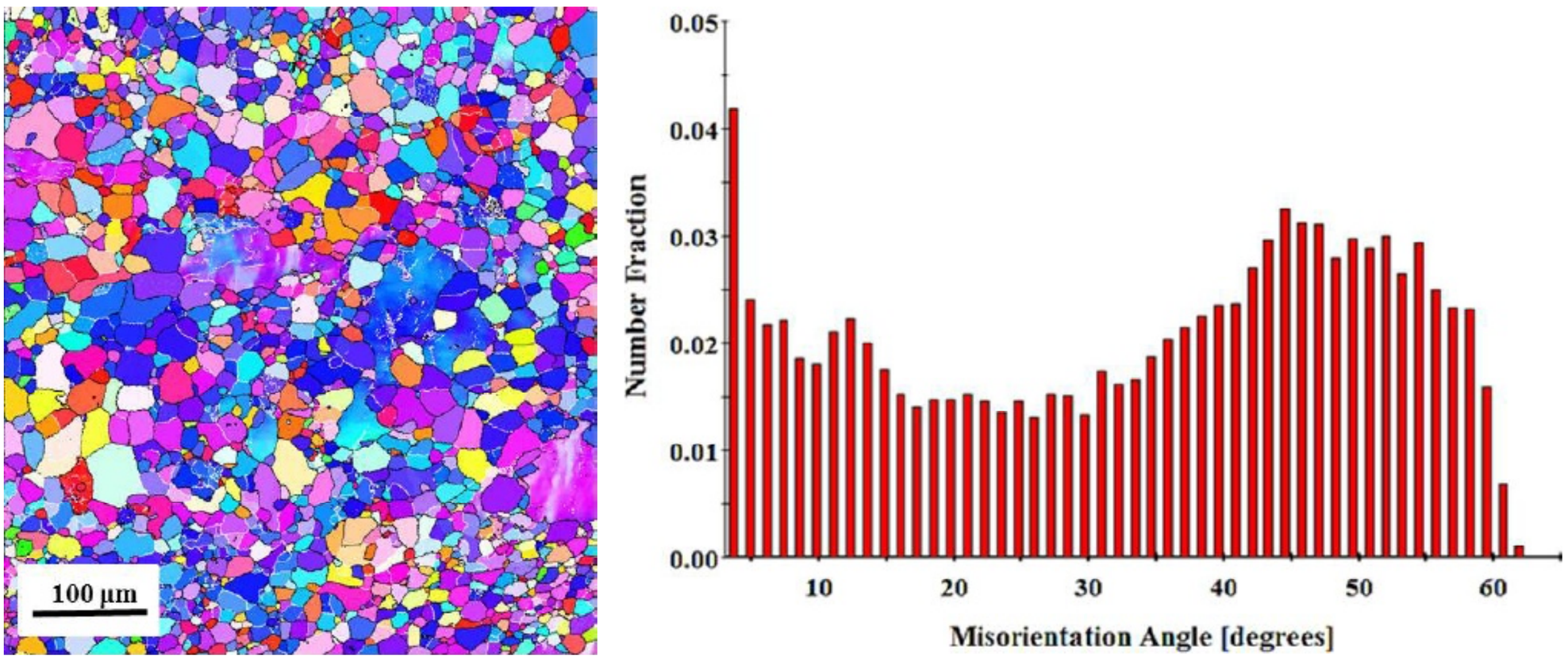

Fig. 3. EBSD grain map (high and low angle grain boundaries are identified by black and white markers, respectively) and the grain boundary misorientation distribution for Ti–26Nb–7Mo–12Zr alloy after rolling at 60% reduction and subsequent annealing at T = 850 °C before quenching.

the analysis by EBSD (Fig. 2), large deformed (initial) grains are prevailing in the state 1 of the structure. During annealing the formation and growth of recrystallization nuclei occur at the initial grain boundaries. The recrystallization process is almost completed in the material as the deformation degree increases up to 60%. Some unrecrystallized areas are still retained in the structure (see Fig. 3). The average grain size of the investigated alloy after rolling at 30% reduction with a subsequent annealing before quenching is about 20.5 μm, while for state 2 it is about 10 μm. As the result of rolling with

Table 1. Characteristics of Ti–26Nb–7Mo–12Zr alloy.

Ti–26Nb–7Mo–12Zr	V_{RG}, %	V_{HAGB}, %	ρ, g/cm^3	E, GPa	δ×10^{-5}	σ, MPa
Initial state	–		5.71	80.7	212	14
state 1	43	37	5.68	71.1	298	9
state 2	94	78	5.72	75.1	275	12
state 3	100	82	5.78	86.4	67	22

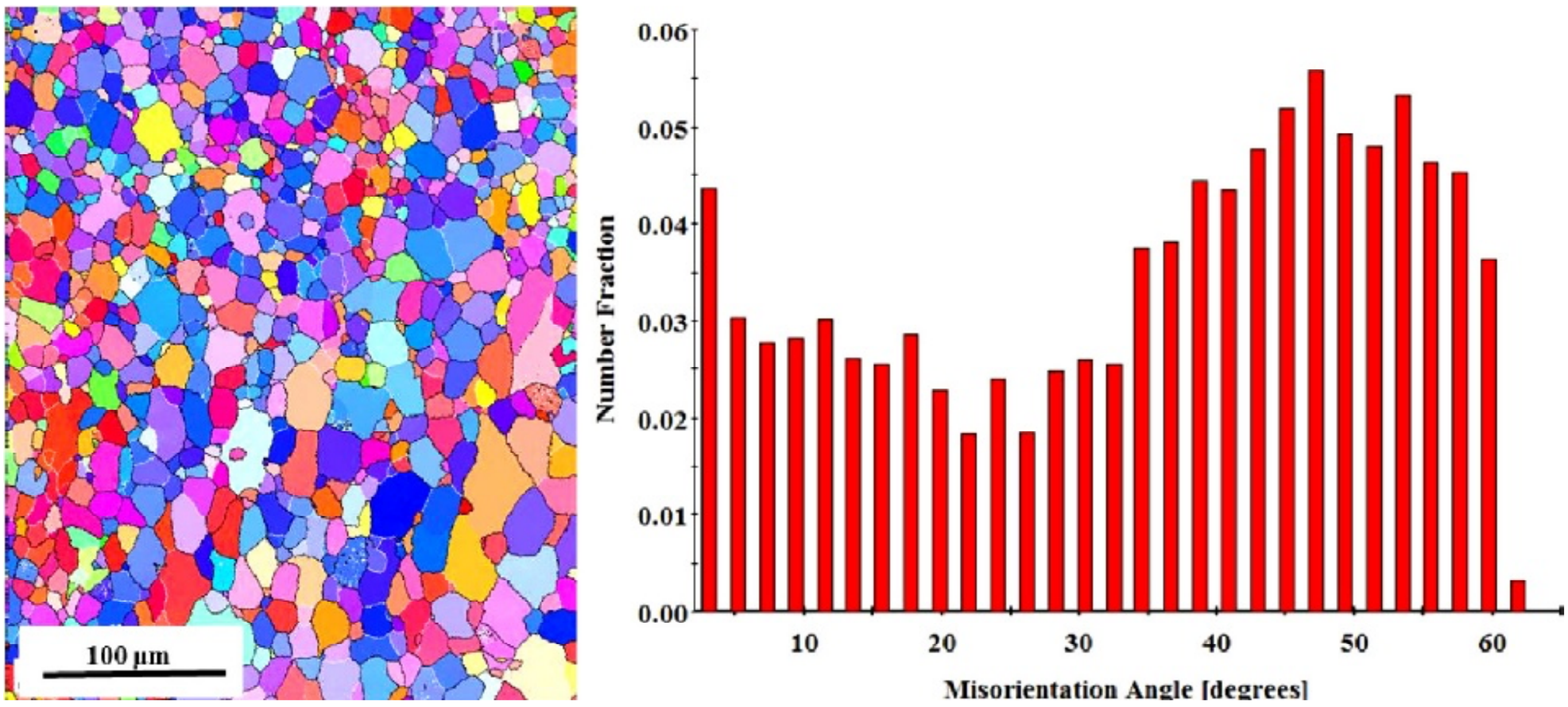

Fig. 4. EBSD grain map (high and low angle grain boundaries are identified by black and white markers, respectively) and the grain boundary misorientation distribution for Ti–26Nb–7Mo–12Zr alloy after rolling at 90% reduction and subsequent annealing at T = 850 °C before quenching.

the maximum degree of deformation, recrystallization occurred throughout the sample volume during high temperature annealing in contrast to the other states (with a lower deformation degree). The increase in the deformation degree leads to the formation of a 9-μm homogeneous fine-grained globular structure with a fraction of high angle grain boundaries (V_{HAGB}) of about 82% (Fig. 4, Table 1).

As mentioned above, the elastic modulus is an important functional characteristic for biomedical metal materials. A correct estimation of elastic modulus by modern research methods is an actual practical problem. There are two groups of methods for elastic modulus measurement: static and dynamic. In contrast to static methods, the dynamic methods (acoustic resonance method, reverse torsion pendulum, nanoindentation) do not lead to a sample destruction or structure change of the material under study. These measurements were carried out in a linear viscoelastic region at low stresses and strains. We determined the elastic modulus by using the exact non-destructive acoustic method [34].

Elastic modulus E and also amplitude independent decrement ratio δ and microyield stress σ were measured by the acoustic resonance method including a piezoelectric vibrator at longitudinal vibrations with a 100 kHz resonance frequency. The measurements of elastic modulus E and amplitude-independent decrement ratio δ were carried out in a wide vibrational strain amplitude range ε. We used moderate amplitudes for retaining the dislocation structure of the samples. Moreover, the dislocation density of the samples remained unchanged after the acoustic method is applied [35]. The elastic modulus was calculated by the following formula:

$$E = 4\rho l^4 f, \qquad (1)$$

where l is the sample length, ρ is the sample density, and f is the vibration frequency.

The sample density ρ was determined by a precise hydrostatic weighing method. The Ti–26Nb–7Mo–12Zr alloy samples were $30 \times 3 \times 0.6$ mm^3 in size and had a weight of 0.3 g. The relative error in determining the density $\Delta\rho/\rho$ did not exceed 0.01%. Table 1 shows average densities obtained for each state of the samples. The sample densities are seen to increase from 5.68 to 5.78 g/cm^3 with increasing deformation degree.

Results of sample density measurements were used according to Eq. (1) to determine the elastic modulus. Figs. 5 and 6 show elastic modulus E and decrement ratio of elastic vibrations σ as functions of amplitude ε. These dependences were successively measured at increasing and decreasing amplitudes. An amplitude hysteresis is visible in all cases: the curves recorded at increasing and decreasing amplitude do not coincide. However, the shape of hysteresis and numerical values of elastic modulus and decrement ratio depend on the degree of deformation at thermomechanical processing. The minimum value of the elastic modulus is observed in state 1 (30% degree of deformation) with a partially recrystallized structure (Table 1, Fig. 5a). State 3 with a fully recrystallized structure has the maximal elastic modulus (see Table 1 and Fig. 5c).

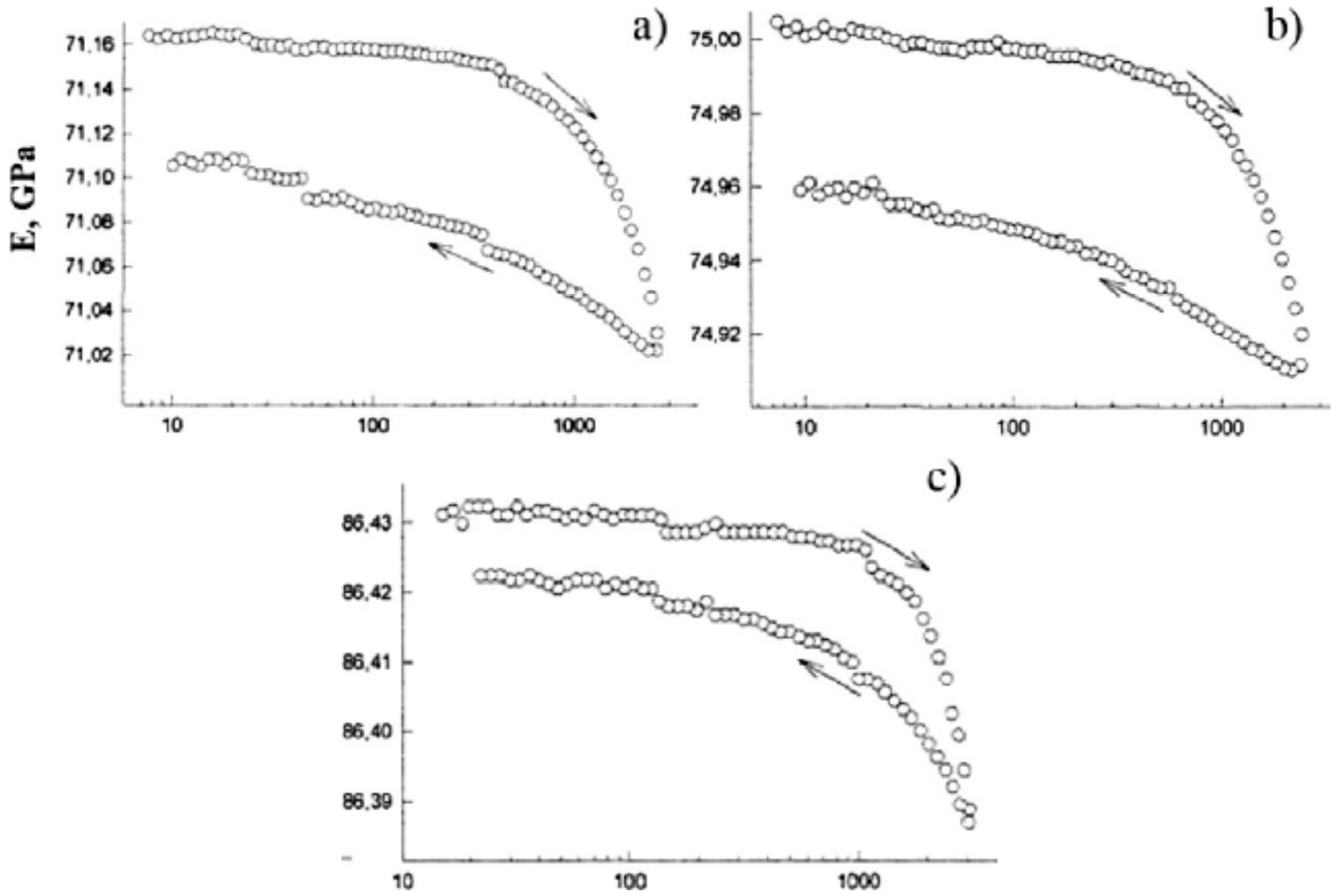

Fig. 5. Amplitude dependences of elastic modulus of Ti–26Nb–7Mo–12Zr alloy after rolling at reduction by 30% (a), 60% (b), and 90% (c) and subsequent annealing at T = 850 °C before quenching that were sequentially measured for increasing and decreasing amplitude ε (the arrows show the direction of change in e). T = 20 °C.

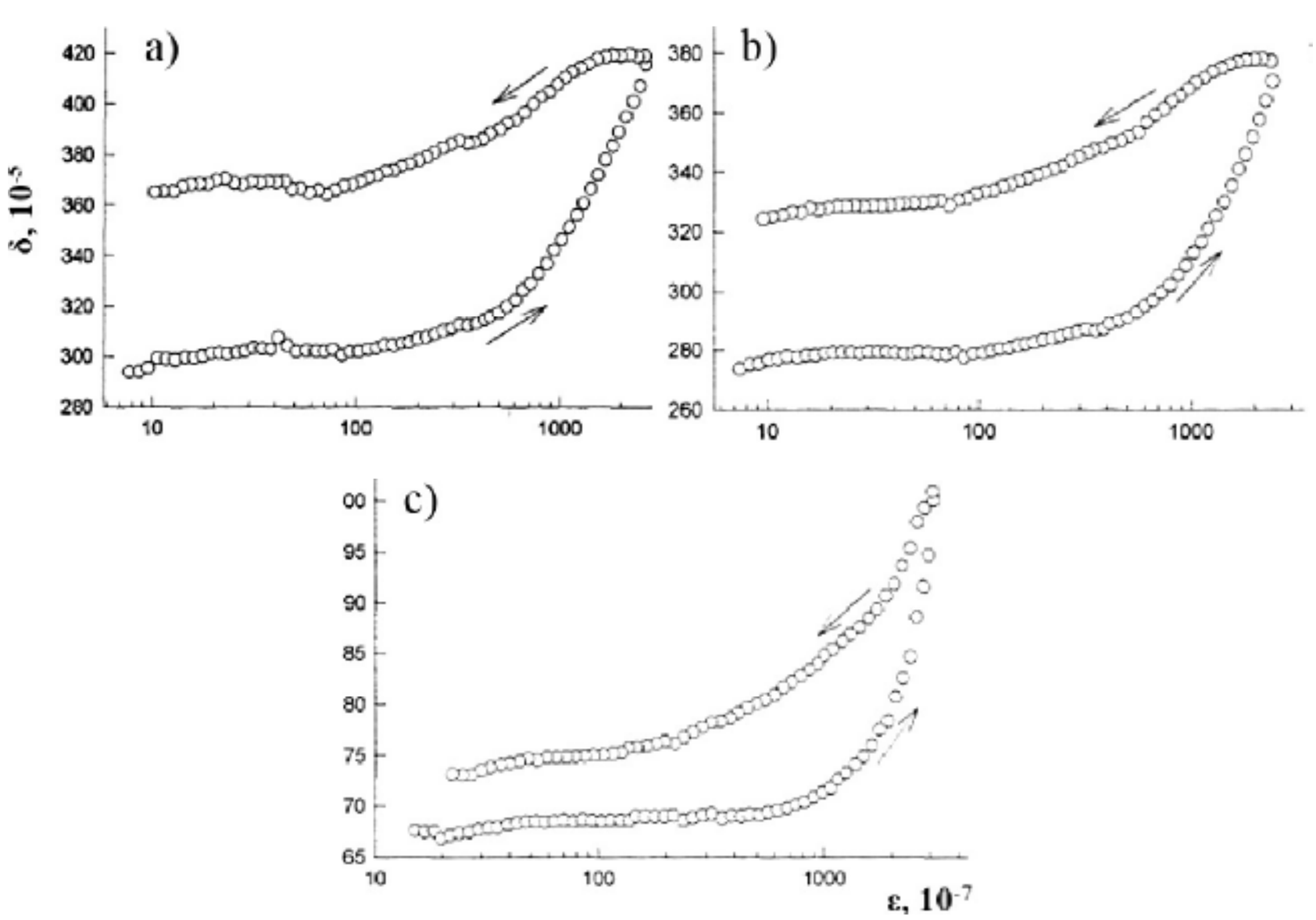

Fig. 6. Amplitude dependences of the damping ratio of Ti–26Nb–7Mo–12Zr alloy after rolling at reduction by 30% (a), 60% (b), and 90% (c) and subsequent annealing at T = 850 °C before quenching that were sequentially measured for increasing and decreasing amplitude e (the arrows indicate the direction of change in ε). T = 20 °C.

It is known that elastic modulus and decrement ratio measured with a high accuracy are structure-sensitive parameters of the material. Further, elastic modulus decreases and decrement ratio increases with increasing dislocation density according to the theory considering the interaction of dis-

locations with point defects. This corresponds to the data obtained in [35,36]. The samples which preserved deformation-induced unrecrystallized defective areas with a high density of dislocations and low angle grain boundaries exhibited a decrease in the elastic modulus relative to the initial state (80.7 GPa) and a decrement ratio increase (see Table 1). The increase in the recrystallized grain volume fraction V_{RG} leads to an increase in the elastic modulus and reduction in the decrement ratio. Such a behavior of elastic modulus and decrement ratio can be attributed to the formation of the defect free recrystallized structure. It is confirmed by the following equation for the decrement ratio δ [35]:

$$\delta \sim b\lambda l^4, \qquad (2)$$

where λ is the dislocation density, l is the length of the dislocation segment, b is the material constant. This equation shows that the value of decrement ratio decreases with the dislocation density reduction. According to [37], long range internal stress fields (through higher order elastic constants) can influence on the measured elastic modulus. Sources of these stresses in metallic materials with a microcrystalline structure are nonequilibrium high angle grain boundaries, triple junctions and other defects of crystal structure. Indeed, as structural studies showed (Figs. 2–4, Table 1), the fraction of grain boundaries with a large misorientation ($\geq 15°$) significantly increases with the increasing deformation degree. From this point of view, as shown in [34], the formation of nonequilibrium high angle grain boundaries (78–82%) leads to high internal stresses that influence on the change in the elastic modulus. Noteworthy is the following result: the increase in the fraction of high angle grain boundaries V_{HAGB} almost in 2 times (from 37% in state 1 to 78% in state 2) led to a growth of the modulus by 6%. However, an insignificant increase in V_{HAGB} from 78 to 82% leads to a substantial increase of the elastic modulus by 15%.

The reduction in the elastic modulus also takes place at the formation of regions of an excess free volume like nanopores [38]. From this viewpoint, the elastic modulus significantly decreases for state 1 in comparison with the initial one. This can be explained by a high concentration of low porosity regions. Therefore, the density value is an indicator of the defect level caused by nanoporosity, dislocation density, misorientation of boundaries and other features. The link between the porosity and elastic modulus is especially pronounced at the deformation degree increase from 30 to 90% that leads to an increase in the alloy density and, as a result, a significant rise in the elastic modulus.

The formation of the recrystallized fine grained structure also explains the increase in the microplastic flow stress σ. Microplastic properties described in [34] were obtained from elastic modulus E and decrement ratio of elastic vibrations δ measured over a wide vibrational strain amplitude range ε, when a nonlinear amplitude dependent absorption $\delta_n = \delta - \delta_i$ and amplitude dependent defect of elastic modulus $(\Delta E/E)_n = (E - E_i)/E_i$ appear in the material at large values of ε. Here, E_i and δ_i are the elastic modulus and decrement ratio measured at low amplitudes, where the modulus E and decrement ratio δ are independent of ε. Acoustic measurements allow us to estimate microplastic properties of materials and plot stress-inelastic strain diagrams in a wide amplitude range. In these diagrams, the ordinates are amplitudes of vibrational stresses $\sigma = E\,\varepsilon$ and the abscissa is nonlinear inelastic strain $\varepsilon_d = \varepsilon(\Delta E/E)_n$. Microyield stress $\sigma = \sigma_s$ was determined at inelastic strain ε_d on the order of 10^{-7} from the constructed diagrams of dependences $E(\varepsilon)$ taken at the first increase in the amplitude (Fig. 7, Table 1). The maximum value of the microyield stress is 22 MPa in state 3 with the fully recrystallized structure in comparison with states (1 and 2) with partially recrystallized structures. The

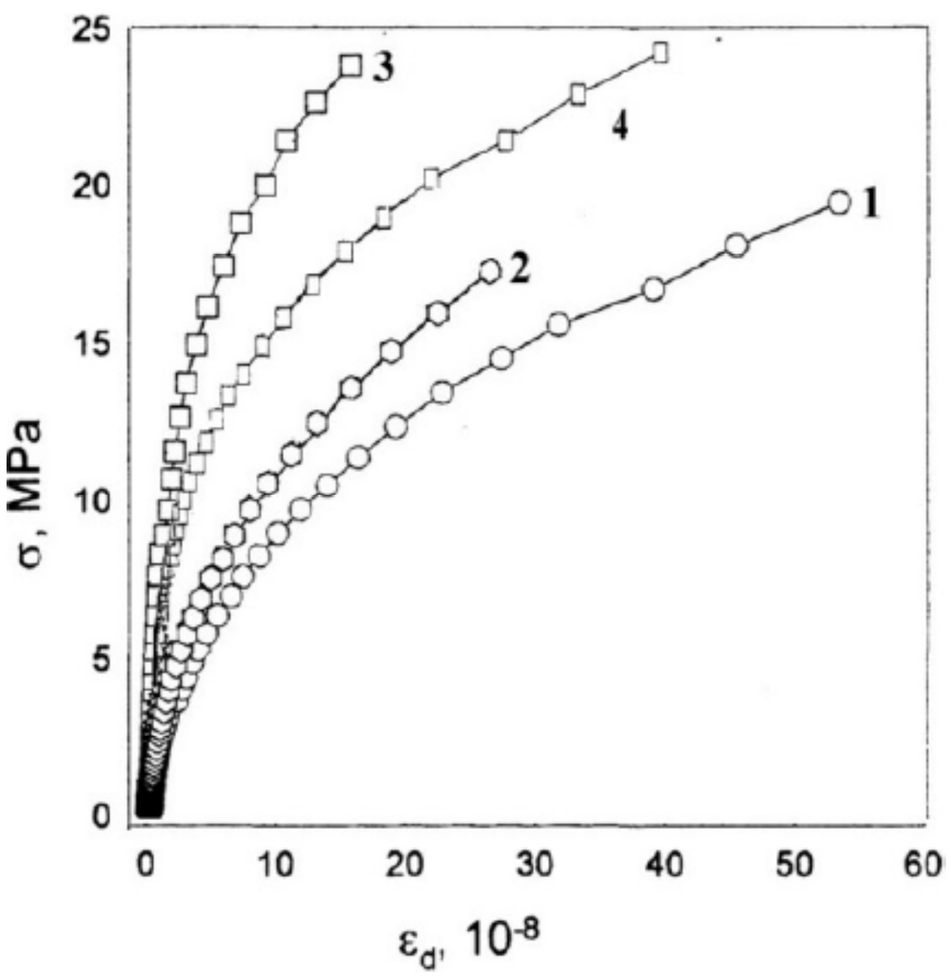

Fig. 7. Stress–microplastic strain curves plotted from acoustic measurements for Ti–26Nb–7Mo–12Zr alloy after rolling at reduction by 30% (1), 60% (2), and 90% (3) followed by annealing at T = 850 °C before quenching; and for the initial state (4); T = 20 °C.

Table 2. Mechanical properties of Ti–26Nb–7Mo–12Zr alloy.

Ti–26Nb–7Mo–12Zr	$\sigma_{0.2}$, MPa	UTS, MPa	Plasticity, %
Initial state	793±5	800±6	6.3±0.2
state 1	755±1	757±1	5.5±2.1
state 2	767±3	768±2	7.1±0.8
state 3	754±7	759±7	8.5±1.2

Table 3. Chemical composition of titanium alloys VT1–0.

Alloy	The content of elements, wt.%, Ti base									
	Al	Mo	V	Zr	Fe	Si	O_2	C	N_2	H_2
VT1–0	0.01	-	-	-	0.12	0.002	0.143	0.004	0.003	0.0008

microyield stress in the initial state of the investigated alloy (14 MPa) is higher than the corresponding value for states 1 and 2 with the partially recrystallized structure, but almost in two times less than the value in state 3 with the fully recrystallized structure. It should be stressed that the formation of the defect free (equilibrium) ultrafine grain recrystallized structure leads to a significant increase in both microplastic properties (microyield stress) and elastic modulus. The alloy with a predominantly deformed matrix (in this case the fraction of recrystallized grains is less than 50%) is characterized by lower values of elastic modulus and microyield stress.

3. LOW MODULUS TITANIUM β-ALLOY Ti–26Nb–7Mo–12Zr: DURABILITY, MECHANICAL, CORROSIVE AND TRIBOLOGICAL PROPERTIES.

It is known that the functional reliability of medical implants and constructions depend on several mechanical properties which manifest themselves under real working conditions in living organisms. In connection with this, along with mechanical characteristics of metals, such as strength and plasticity, the durability, resistance to corrosion and wearing capacity are important [1].

Testing of the mechanical properties of the Ti–26Nb–7Mo–12Zr alloy in the initial coarse grained state shows that the ultimate tensile strength (UTS) and yield strength ($\sigma_{0.2}$) are about 800 MPa. Note that the most widely used titanium alloy VT6 (Ti–4Al–6V) possesses a high strength of 950 MPa and a sufficiently high plasticity of about 12–16%. However, the main disadvantage of this alloy is vanadium alloying. As one can see from Table 2, the strength characteristics were slightly decreased after thermomechanical processing, while the plasticity was increased by 2% as compared with the initial state.

In the present study, constant load creep tests of the low modulus titanium alloy were conducted in tension. All of the tests were continued up to the final fracture. Commercially pure titanium VT1–0 (the content of impurity is shown in Table 3) with an average grain size of about 6 μm was used for comparison with the low modulus β-type alloy.

The durability of the Ti–26Nb–7Mo–12Zr alloy with a coarse-grained structure (initial state) and VT1–0 alloy was estimated on the basis of creep tests. Standard creep curves for α- and β-type titanium alloys are shown in Fig. 8. All of these plots were obtained at a temperature of 400 °C and an applied tensile stress of 300 MPa. As one can see, the β-type titanium alloy exhibits higher characteristics of durability. As demonstrated by the creep curves in Fig. 8, the creep life (the time to fracture) of the β-type alloy exceeds by more than two orders of magnitude the corresponding value for the CP titanium.

The standard creep curves (Fig. 8) were replotted in the form of the creep rate vs. time and the creep rate vs. strain, as shown in Figs. 8b and 8c. It follows from Figs. 8b and 7c that the creep rate for the unalloyed titanium VT1–0 is higher than for the Ti–26Nb–7Mo–12Zr alloy.

It is known that wear is a critical process in the use of an implant that determines its lifetime in a living organism. A low wear resistance of an implanted material can lead to various adverse consequences for a living organism [15]. It is interesting to note that titanium and its alloys have low tribo-

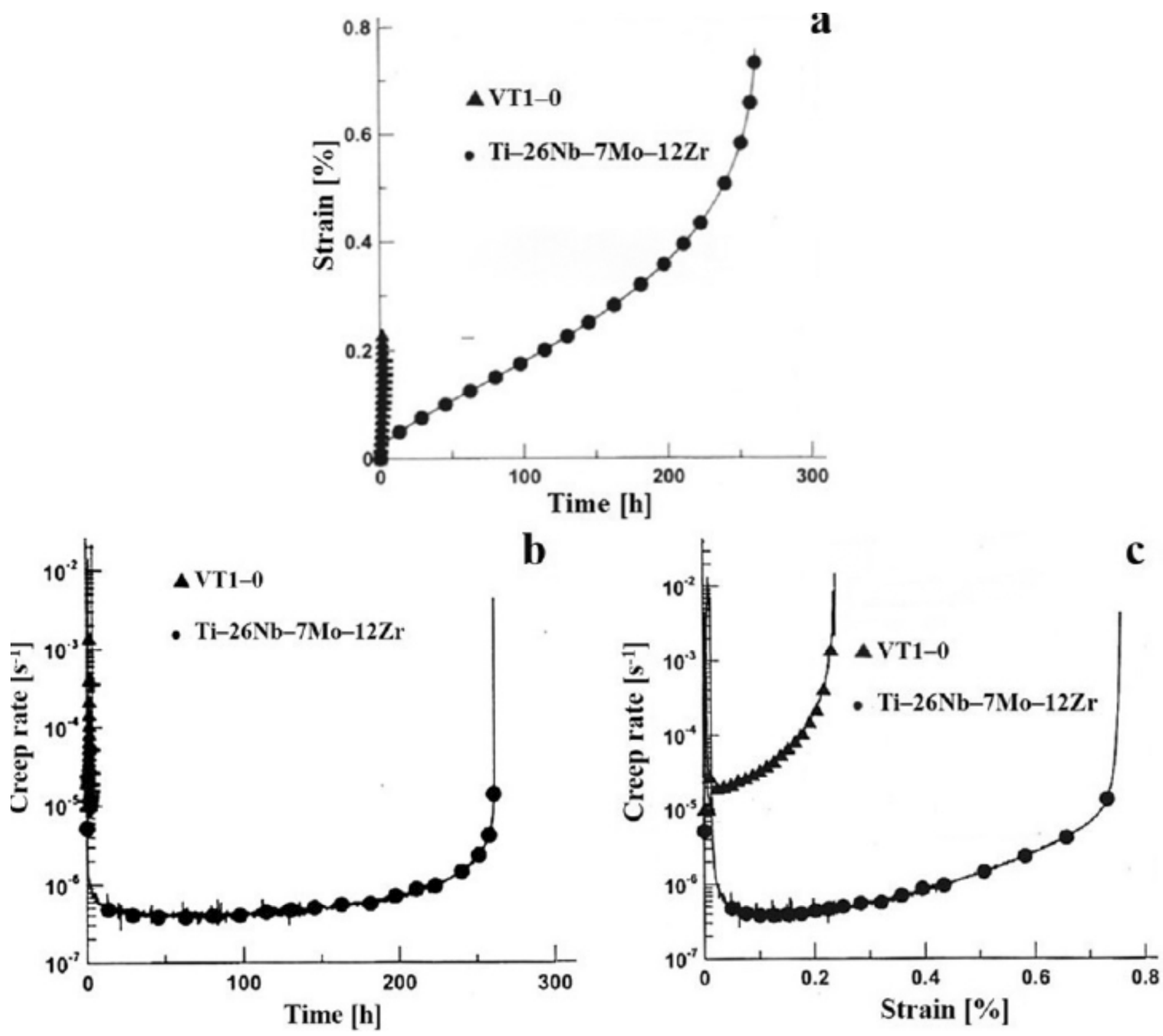

Fig. 8. Creep curves for CP Ti VT1–0 and Ti–26Nb–7Mo–12Zr alloy.

logical characteristics in pairs "metal-metal" due to a high propensity to frictional seizure. This phenomenon is promoted by low values of the elastic modulus and a low thermal conductivity.

Table 4 shows the wear factor values obtained at wear tests for the samples of the Ti–26Nb–7Mo–12Zr alloy and rider. Analogous investigations of unalloyed titanium VT1–0 and VT6 alloy were conducted for comparison with the low-modulus alloy. These investigations have shown higher characteristics of wear resistance for the Ti–26Nb–7Mo–12Zr alloy as compared to VT1–0 and VT6. The wear factor of unalloyed titanium VT1–0 and alloy VT6 exceeds in more than in 2 times the corresponding values for the alloy under study. This is probably connected with a high content of niobium in this alloy. The addition of this element into titanium alloys leads to a quick passivation of the alloy surface, and the formed oxide of niobium (Nb_2O_5) possesses good lubricating properties according to the published data [6].

It is interesting to note that the Ti-26Nb-7Mo-12Zr alloy in the initial state and with a predominantly deformed matrix is found to exhibit a high wear resistance as compared to the state 3 with the homogeneous fine-grained structure.

The β-type titanium alloy, like the β-type and (α + β)-type titanium alloys widely used in medicine, demonstrates a high corrosion resistance. This is probably due to the fact that the oxides of alloying elements, especially Nb and Zr, formed on the surface of the alloy according to [6,39-41] increase the corrosion resistance of titanium alloys.

Investigations of the surface by scanning electron microscopy have shown [21] that all the states of the Ti–26Nb–7Mo–12Zr alloy studied are charac-

Table 4. Wear factor of titanium alloys and rider.

	Ti–26Nb–7Mo–12Zr				VT1–0	VT6
	Initial state	state 1	state 2	state 3		
Wear factor, 10^{-4} $mm^3/N^{-1}\cdot m^{-1}$	1.8	1.6	2.0	2.1	4.3	5.3
Wear factor of rider, 10^{-5} $mm^3/N^{-1}\cdot m^{-1}$	1.4	1.2	1.2	1.2	2.0	2.4

terized by deep spot destructions after anodic polarization. These destructions point to a pitting corrosion. It is known that the development of pitting corrosion is promoted by various structural defects, such as grain boundaries and subgrains, dislocation clusters, secondary dispersed separation and phase.

4. CONCLUSIONS

Complex investigations of the microstructure and its influence on strength and elastic-microplastic properties of the new developed titanium alloys system Ti–Nb–Mo–Zr with a low elastic modulus, a high resistance to corrosion and wear have been carried out.

Experimental data and their analysis showed that the formation of the partially recrystallized (predominating defective) structure of the Ti–26Nb–7Mo–12Zr alloy leads to a reduction in elastic modulus and microyield stress and an increase in the decrement ratio.

The formation of the fully recrystallized structure leads to increases in the values of elastic modulus, microyield stress and plasticity as compared with the coarse grained and partially recrystallized states, while the decrement ratio is significantly reduced.

It was found that the creep life of Ti–26Nb–7Mo–12Zr alloy is more than 250 hours at temperature of 400 °C and stress of 300 MPa, while the creep life of unalloyed titanium VT1–0 is only 2 hours under the same creep loading conditions.

ACKNOWLEDGEMENT

The study was supported by a grant from the Russian Science Foundation (project ¹ 15-12-30010).

REFERENCES

[1] Yu. R. Kolobov // *Nanotechnology in Russia* **4** (2009) 758.
[2] J.Y. Wong and J.D. Bronzino, *Biomaterials* (Taylor & Francis Group, USA, 2007).
[3] B. Gunawarman, M. Niinomi, T. Akahori, T. Souma, M. Ikeda and H. Toda // *Mat. Sci. and Eng. C* **2**5 (2005) 304.
[4] M. Niinomi, M. Nakai and J. Heida // *Acta Biomaterials* **8** (2012) 3888.
[5] B.D. Ranter, A.S. Hoffman, F.J. Schoen and J.E. Lemons, *Biomaterials Science: An Introduction to Materials in Medicine*, 2 ed. (Elsevier Academic Press, San Diego, 2004).
[6] M. Geetha, A.K. Singh, R. Asokamani and A.K. Gogia // *Progress in materials science* **54** (2009) 397.
[7] D.R. Peterson and J.D. Bronzino, *Biomechanics Principles and Applications* (Taylor & Francis Group, USA, 2008).
[8] C.M. Agrawal // *JOM* **50** (1998) 31.
[9] R. Godley, D. Starosvetsky and I. Gotman // *J. Mater. Sci. Mater. Med.* **17** (2006) 63.
[10] R. Thull // *Naturwissenschaften* **81** (1994) 481.
[11] J. Malek, F. Hnilica, J. Vesely, B. Smola, S. Bartakova and J. Vanek // *Mater. Des.* **35** (2012) 731.
[12] S.F. Ou, H.H. Chou, C.S. Lin, C.J. Shih, K.K. Wang and Y.N. Pan // *Appl. Surf. Sci.* **258** (2012) 6190.
[13] K. Wang // *Mater. Sci. Eng. A* **213** (1996) 134.
[14] C.M. Lee, W.F. Ho, C.P. Ju and J.H. Chern-Lin // *J. Mater. Sci. Mater. Med.* **13** (2002) 695.
[15] T. Hanawa, S. Hiromoto and A. Yamamoto // *Structural biomaterials for the 21 century* (2001) 145.
[16] S. Ankem and C.A. Greene // *Mater. Sci. Eng. A* **263** (1999) 127.
[17] I. Weiss and S.L. Semiatin // *Mater. Sci. Eng. A* **243** (1998) 46.
[18] R. Banerjee, S. Nag and H.L. Fraser // *Mater. Sci. Eng. C* **25** (2005) 282.
[19] Long Marc and H.J. Rack // *Biomaterials* **19** (1998) 1621.
[20] M. Niinomi // *Science and technology of advanced materials* **4** (2003) 445.
[21] O.A. Golosova, M.B. Ivanov, Yu.R. Kolobov and T.N. Vershinina // *Mat. Sci. and Tech*. **29** (2013) 204.
[22] L. Khench and D. Dzhons, *Biomaterials, artificial organs and tissue engineering* (Technosphere, Moscow, 2007).
[23] M. Niinomi // *JOM* **51** (1999) 32.
[24] H. Kawahara // *Bulletin of the Japan Institute of Metals* **31** (1992) 1033.
[25] Y. Okazaki, S. Rao, Y. Ito and T. Tateishi // *Biomaterials* **19** (1998) 1197.
[26] M. Nakai, M. Niinomi and T. Akahori // *Advances in Materials Research* **10** (2008) 167.
[27] M. Morinaga, M. Kato, T. Kamimura, M. Fukumoto, I. Harada and K. Kubo, In: *Titanium 92: science and technology*, ed. by F. H. Frees and I. Caplon (Warrendale: The Minerals, Metals & Materials Society, 1992).

[28] X. Song, L. You, B. Zhang and A. Song // *Mat. Tech.* **27** (2011) 334.
[29] K. Cho, M. Niinomi, M. Nakai, J. Hieda and Y. Kawasaki // *Mat. Trans.* **54** (2013) 574.
[30] D-S. Bae, S-J. Jang, H. Yukawa, Y. Murata and M. Morinaga // *Mat. Trans.* 42 (2001) 1112.
[31] M. Morinaga, Y. Murata and H. Yukawa // *J. Mat. Sci. Technol.* **19** (2003) 73.
[32] K. Matsugi, Y. Murata, M. Morinaga and N. Yukawa // *Mat. Sci. Eng. A* **172** (1993) 101.
[33] J.S. Zhang, Z.Q. Hu, Y. Murata, M. Morinaga and N. Yukawa // *Metallurgical Transactions* **24** (1993) 2443.
[34] V.I. Betekhtin, Yu.R. Kolobov, O.A. Golosova, B.K. Kardashev, A.G. Kadomtsev, M.V. Narykova, M.B. Ivanov and T.N. Vershinina // *Technical Physics* **58** (2013) 1432.
[35] S.P. Nikanorov and B.K. Kardashev, *Elasticity and dislocation inelasticity of crystal* (Science, Moscow, 1985).
[36] G. Gremaud // *Mat. Sci. Forum* **366** (2001) 178.
[37] V.I. Betekhtin, A.G. Kadomtsev and B.K. Kardashev // *Physics of the Solid State* **48** (2006) 1506.
[38] V.I. Betekhtin, Yu.R. Kolobov, M.V. Narykova, B.K. Kardashev, E.V. Golosov and A.G. Kadomtsev // *Technical Physics* **56** (2011) 1599.
[39] M.A. Khan, R.L. Williams and D.F. Williams // *Biomaterials* **17** (1996) 2117.
[40] Y. Okazaki, E. Nishimura, H. Nakada and K. Kobayashi // *Biomaterials* **22** (2001) 599.
[41] A. Kawashina, S. Watanabe, K. Asami and S. Hanada // *Mater. Trans*. **44** (2003) 1405.